A Global State Observer-Based Open-Switch Fault Diagnosis for Bidirectional DC–DC Converters in Hybrid Energy Source System

Jun Hang, *Member, IEEE*, Chaoqiang Ge, Shichuan Ding, *Member, IEEE*, Wei Li, *Member, IEEE*, Yourui Huang, and Wei Hua, *Senior Member, IEEE*

***Abstract*—Open-switch fault is one of the most common faults of dc–dc converter. If the fault cannot be diagnosed in time, it will have a serious impact on the normal operation of the system. To solve this problem, this article proposes an open-switch fault diagnosis method for bidirectional dc–dc converter based on global state observer. In this method, the global mathematical model of two bidirectional dc–dc converters in hybrid energy sources system is first derived, and then a global state observer is constructed based on Luenberger observer. The open-switch fault detection and location are achieved through the residuals of battery current and supercapacitor current. Both the simulation and experimental results verify the effectiveness of the proposed open-switch fault diagnosis method.**

***Index Terms*—Bidirectional dc–dc converter, global state observer, open-switch fault diagnosis, residual signals.**

I. Introduction

NOWADAYS, the hybrid energy source-fed permanent magnet motor system is widely used for electric vehicles, which mainly includes a hybrid energy source system (HESS) (battery, supercapacitor, and two bidirectional dc–dc converters, also called interface circuits) and a permanent magnet synchronous motor (PMSM) [1], as shown in Fig. 1. The HESS composed of batteries and supercapacitors commonly adopts an active structure: the batteries and supercapacitors are, respectively, connected to the dc bus through two bidirectional dc–dc converters, which can give full play to the advantages of HESS.

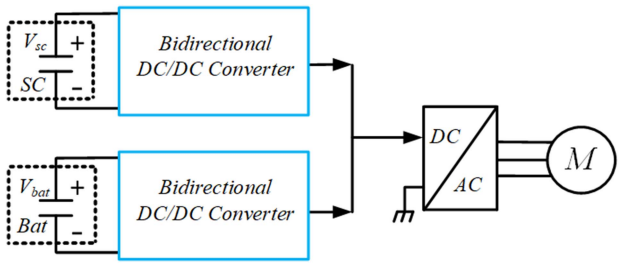

Fig. 1. Hybrid energy source fed PMSM system.

For the HESS, the dc–dc converters are the most prone to the failures, and the faults mainly include power tubes faults, capacitor faults, and interface faults [2], [3]. Among them, power switch faults account for about 31%, mainly including open-circuit fault and short-circuit fault. The short-circuit fault evolves rapidly and is usually converted into open-circuit fault by adding fast fuses in the converter [4]. The open-circuit fault of the power switch will inevitably affect the control function of the converter. If the fault is not detected in time, the fault will reduce the reliability of the system, and even lead to the secondary failure, thus causing the paralysis of the entire system. Hence, it is of great significance for fault diagnosis of power switch in HESS to ensure the safe operation of electric vehicles.

Up to now, a few open-switch fault diagnosis methods have been presented for dc–dc converter, which are mainly based on inductor current [5], [6], [7], [8], [9], inductor voltage [10], [11], [12], [13], magnetic near-field signal [14], the voltage across devices [15], diode voltage [16], input current [17], [18], module output voltage [19], midpoint voltage [20], and capacitance current derivative [21]. In [5], [6], [7], [8], and [9], the open-circuit faults of the power switch are identified based on the shape of the inductor current. In [10], [11], [12], and [13], the inductor voltage signal is collected by adding an additional auxiliary coil, and the inductor voltage is compared with the timing of the switching device drive signal for real-time fault detection. In [14], a magnetic near-field probe is used to capture the low-frequency and high-frequency magnetic fields

Manuscript received 19 March 2023; revised 10 June 2023; accepted 22 June 2023. Date of publication 29 June 2023; date of current version 1 September 2023. This work was supported in part by the National Natural Science Foundation of China under Grants 52177027, 52107034, and 51607001, in part by Excellent Youth Project of Natural Science Foundation of Anhui Province under Grant 2108085Y18, in part by Key Project of Excellent Young Talents in University of Anhui Province under Grant gxyqZD2021090, and in part by Anhui Provincial Major Science and Technology Project under Grant 202203c08020010. Recommended for publication by Associate Editor A. Safaee. *(Corresponding author: Shichuan Ding.)*

Jun Hang, Chaoqiang Ge, Shichuan Ding, and Wei Li are with the School of Electrical Engineering and Automation, Anhui University, Hefei 230601, China, and also with the National Engineering Laboratory of Energy-Saving Motor and Control Technique, Anhui University, Hefei 230601, China (e-mail: jun_hang511@163.com; 2669446739@qq.com; dingsc@126.com; liwei001x@163.com).

Yourui Huang is with the School of Electrical and Information Engineering, Anhui University of Science and Technology, Huainan 232001, China (e-mail: hyr628@163.com).

Wei Hua is with the School of Electrical Engineering, Southeast University, Nanjing 210096, China (e-mail: huawei1978@seu.edu.cn).

Color versions of one or more figures in this article are available at https://doi.org/10.1109/TPEL.2023.3290603.

Digital Object Identifier 10.1109/TPEL.2023.3290603

near the converter, and fault classification is achieved through a neural network. In [15], the voltage across power devices in dual-active bridge converters is monitored in real-time to detect the open-switch faults. In [16], for nonisolated dc–dc converters, a fault diagnosis method is discussed for switching and diode by sampling diode voltage and gate drive signal. In [17], for the interleaved dc–dc converter, the input current derivative sign characteristic is used for fault diagnosis. In [19], a fault diagnosis method is discussed by sampling the module output voltage via a dedicated hardware circuit. In [20], based on the resonant phenomenon during the fault condition, an open-circuit fault diagnosis strategy that uses midpoint voltage as diagnosis criteria is proposed for dual-active bridge converters. In [21], the capacitor current is sampled by a PCB Rogowski coil and its derivative is used as the signature for fault detection. However, the existing fault diagnosis methods are limited to specific dc–dc converters, such as nonisolated single-tube converters (buck converters or boost converters), interleaved boost converters, cascaded buck converters, series-parallel forward dc–dc converters, modular dc–dc converters. Moreover, the additional sensors or probes are required, which will increase the complexity of the system and the cost of the fault diagnosis.

The bidirectional dc–dc converter has two operating modes: buck and boost. Combined with the operating conditions of electric vehicles, the structure and operating mode of the bidirectional dc–dc converter are different from those of dc–dc converters in [5], [6], [7], [8], [9], [10], [11], [12], [13], [14], [15], [16], [17], [18], [19], [20], and [21]. Therefore, the open-switch fault diagnosis of bidirectional dc–dc converters in HESS cannot be effectively solved by directly applying the previous fault diagnosis methods or by simply combining the previous fault diagnosis methods (fault diagnosis methods for buck converters and boost converters).

At present, the fault diagnosis of bidirectional dc–dc converter is less involved. In [22] and [23], the fault diagnosis method based on state estimation is studied, and the state observer is only designed for buck or boost mode. However, the HESS contains two bidirectional dc–dc converters. If the fault diagnosis methods in [22] and [23] are directly used for two bidirectional dc–dc converters, four state observers are needed to conduct a comprehensive diagnosis of power switch faults. This will reduce the efficiency of fault diagnosis and increase the workload of fault diagnosis at the same time. Hence, to improve the efficiency and accuracy of fault diagnosis, it is necessary to propose a targeted fault diagnosis method for the bidirectional dc–dc converter.

This article proposes a global state observer-based open-switch fault diagnosis method for two bidirectional dc–dc converters in HESS, where only one state observer is needed. The global mathematical model of two bidirectional dc–dc converters in HESS is first derived. Then, a global state observer based on the linear switching model is constructed. The residuals of battery current and supercapacitor current are used to achieve the open-circuit fault detection and location in two bidirectional dc–dc converters. To demonstrate the effectiveness of the proposed fault diagnosis, a hybrid energy source fed PMSM is built for simulation and experimental verification. In addition, the novelty of the proposed fault diagnosis method is described as follow.

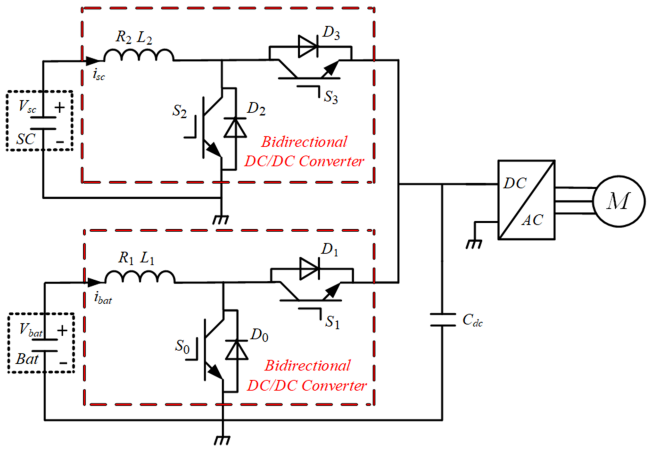

Fig. 2. Topology of bidirectional DC–DC converter in HESS.

1) Aiming at four operating modes of two bidirectional dc–dc converters under hybrid energy source, a global mathematical model is established, and all working states of the whole system can be estimated with only one global observer.
2) It is not necessary to estimate the capacitor voltage of the dc bus, only the battery current and the supercapacitor current is estimated for fault diagnosis.
3) There is no requirement for complex signal processing, and fault location is implemented only based on the estimated current.

The rest of this article is organized as follows. In Section II, the global mathematical model of two bidirectional dc–dc converters in HESS is deduced. In Section III, the open-switch fault diagnosis method is introduced. In Section IV, the simulation research is introduced. In Section V, the experimental implementation is presented. Finally, Section VI concludes this article.

II. Global Mathematical Model of Two Bidirectional DC–DC Converters

A. Topology of Bidirectional DC–DC Converter in HESS

To solve the mismatch problem caused by the different characteristics of two energy sources, the bidirectional dc–dc converter is usually selected as the interface converter used in HESS. Among different bidirectional dc–dc converter topologies, such as bidirectional flyback [24], Cuk [25], push–pull [26], bidirectional forward [27], dual half-bridge [28], and other topologies, the dual half-bridge converter is known owing to its high efficiency (low inductive turn-ON and low switching and conduction losses on the active components [29]) and its wide application in this system [30]. Both the battery and the supercapacitor are connected to bidirectional dc–dc converter and are connected in parallel to the dc bus together, which can realize the independent control of two energy sources and has the strongest adaptability to the load. The topology of the bidirectional dc–dc converter in HESS is shown in Fig. 2.

B. Global Mathematical Model of Two Bidirectional DC–DC Converters

Traditionally, the mathematical model of the bidirectional dc–dc converter for buck mode and boost mode is separately established. As shown in Fig. 2, the HESS contains two bidirectional dc–dc converters. If the traditional modeling method is used, four mathematical models are needed to be established to reflect the operation of the entire system. Hence, in this article, to simplify the mathematical model and improve the efficiency of fault diagnosis, a global mathematical model of two bidirectional dc–dc converters in HESS is established based on the local modeling method. The specific modeling process is given as follows.

1) Local Model Building: The buck mode and boost mode of the bidirectional dc–dc converter correspond to the discharging state and the charging state of the energy source, respectively. Local mathematical models are, respectively, established for two states.

a) Definition of binary switching function: Each energy source contains discharging state and charging state in HESS. To better establish the model, the respective binary switching functions are established according to the charging and discharging states of the battery and the supercapacitor, and are expressed as

$$k=\begin{cases}1 & \text{discharge } (i_{bat,ref}>0)\\ 0 & \text{charge } (i_{bat,ref}<0)\end{cases} \tag{1}$$

$$m=\begin{cases}1 & \text{discharge } (i_{sc,ref}>0)\\ 0 & \text{charge } (i_{sc,ref}<0)\end{cases} \tag{2}$$

where $i_{bat,ref}$ and $i_{sc,ref}$ are the reference values of battery current and supercapacitor current, respectively, k and m are binary switching functions and represent the charging and discharging states of the battery and supercapacitor.

b) Discharging states ($k=1$, $m=1$): The dynamic equation of the power electronic converter is usually established by the linear switching model [31]. According to Kirchhoff's law, the state equations of battery current and supercapacitor current in discharging mode are expressed as(The specific process is shown in Appendix.)

$$\begin{cases}\frac{di_{bat}}{dt}=-(1-d_0)\frac{V_{\rm dc}}{L_1}-\frac{R_1}{L_1}i_{bat}+\frac{V_{bat}}{L_1}\\ \frac{di_{sc}}{dt}=-(1-d_2)\frac{V_{\rm dc}}{L_2}-\frac{R_2}{L_2}i_{sc}+\frac{V_{sc}}{L_2}\end{cases} \tag{3}$$

where i_{bat} and i_{sc} are the currents of the battery and the supercapacitor, respectively, R_1 and R_2 are the circuit wire resistances on the battery side and the supercapacitor side, respectively, d_0 and d_2 are duty cycles of switch tubes S_0 and S_2, respectively, V_{bat}, V_{sc}, and $V_{\rm dc}$ are the battery voltage, supercapacitor voltage and dc bus voltage, respectively.

c) Charging states ($k=0$, $m=0$): Similarly, the state equations of the battery current and supercapacitor current in charging mode are expressed as (The specific process is shown in the Appendix.)

$$\begin{cases}\frac{di_{bat}}{dt}=-d_1\frac{V_{\rm dc}}{L_1}-\frac{R_1}{L_1}i_{bat}+\frac{V_{bat}}{L_1}\\ \frac{di_{sc}}{dt}=-d_3\frac{V_{\rm dc}}{L_2}-\frac{R_2}{L_2}i_{sc}+\frac{V_{sc}}{L_2}\end{cases} \tag{4}$$

where d1 and d3 are duty cycles of switch tubes S1 and S3, respectively.

2) Establishment of Global Mathematical Model: According to the state expressions of the battery and supercapacitor in discharging mode and charging mode, by substituting the switching function into (3) and (4), respectively, the global mathematical model of the battery and supercapacitor in charging and discharging mode are given as

$$\begin{cases}\frac{di_{bat}}{dt}=-\left[k(1-d_0)+(1-k)d_1\right]\frac{V_{\rm dc}}{L_1}-\frac{R_1}{L_1}i_{bat}+\frac{V_{bat}}{L_1}\\ \frac{di_{sc}}{dt}=-\left[m(1-d_2)+(1-m)d_3\right]\frac{V_{\rm dc}}{L_2}-\frac{R_2}{L_2}i_{sc}+\frac{V_{sc}}{L_2}\end{cases}. \tag{5}$$

The first coefficient term on the right side of (5) is defined as the unique control signal of two bidirectional dc–dc converters

$$d_{01}=k(1-d_0)+(1-k)d_1 \tag{6}$$

$$d_{23}=m(1-d_2)+(1-m)d_3. \tag{7}$$

According to (5)–(7), the global mathematical model of two bidirectional dc–dc converters in the HESS can be obtained as

$$\begin{cases}\frac{di_{bat}}{dt}=-\frac{R_1}{L_1}i_{bat}-\frac{d_{01}}{L_1}V_{\rm dc}+\frac{V_{bat}}{L_1}\\ \frac{di_{sc}}{dt}=-\frac{R_2}{L_2}i_{sc}-\frac{d_{23}}{L_2}V_{\rm dc}+\frac{V_{sc}}{L_2}.\end{cases} \tag{8}$$

III. Open-Switch Fault Diagnosis

According to the global mathematical model of two bidirectional dc–dc converters in HESS, a global Luenberger observer is constructed to estimate the battery current and the supercapacitor current. In this article, the open-switch fault of two bidirectional dc–dc converters is detected and located by the residuals of the battery current and the supercapacitor current.

A. Design of Global State Observer

Equation (8) is changed into the description form of the state space equation

$$\begin{cases}\dot{x}(t)=Ax(t)+Bu(t)\\ y(t)=Cx(t)\end{cases} \tag{9}$$

where $A=\begin{bmatrix}-\frac{R_1}{L_1} & 0\\ 0 & -\frac{R_2}{L_2}\end{bmatrix}$, $B=\begin{bmatrix}\frac{1}{L_1} & 0\\ 0 & \frac{1}{L_2}\end{bmatrix}$, $C=\begin{bmatrix}1 & 0\\ 0 & 1\end{bmatrix}$, $x(t)=\begin{bmatrix}i_{bat} & i_{sc}\end{bmatrix}^T$, $u(t)=\begin{bmatrix}V_{bat}-d_{01}V_{\rm dc} & V_{sc}-d_{23}V_{\rm dc}\end{bmatrix}^T$.

Before designing the Luenberger observer, the observability of the system is analyzed. Because the matrix C is full rank, the rank of the observable matrix of the system must be full rank. Hence, the system is completely observable and meets the requirements of the Luenberger observer. In this case, the Luenberger observer is designed as

$$\begin{cases}\dot{\hat{x}}=A\hat{x}+Bu+K_e(y-\hat{y})\\ \hat{y}=C\hat{x}\end{cases} \tag{10}$$

where $\hat{x}$ is the estimated value of state variable x, $\hat{y}$ is the estimated value of output variable y. The gain coefficient matrix K_e is expressed as

$$K_e=\begin{bmatrix}k_{e1} & 0\\ 0 & k_{e2}\end{bmatrix}. \tag{11}$$

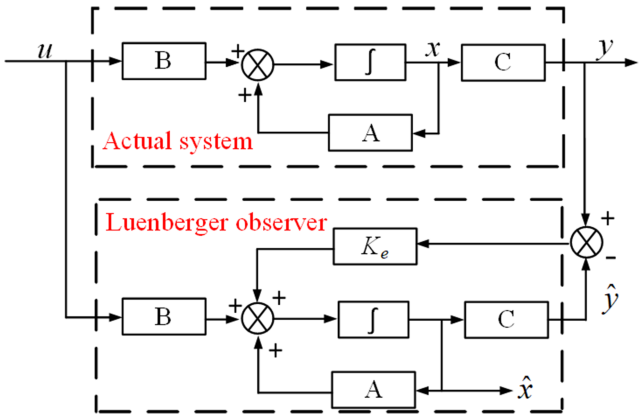

Fig. 3. Block diagram of the observer structure.

As long as the appropriate gain coefficient matrix is selected, the residuals will converge and the rate of convergence can be achieved by adjusting K_e. The block diagram of the state observer and the actual system is shown in Fig. 3, and the designed Luenberger observer is expressed as

$$\begin{bmatrix} \frac{d\hat{i}_{bat}}{dt} \\ \frac{d\hat{i}_{sc}}{dt} \end{bmatrix} = \begin{bmatrix} -\frac{R_1}{L_1} & 0 \\ 0 & -\frac{R_2}{L_2} \end{bmatrix} \begin{bmatrix} \hat{i}_{bat} \\ \hat{i}_{sc} \end{bmatrix} + \begin{bmatrix} \frac{1}{L_1} & 0 \\ 0 & \frac{1}{L_2} \end{bmatrix} \begin{bmatrix} V_{bat} - d_{01}V_{\mathrm{dc}} \\ V_{sc} - d_{23}V_{\mathrm{dc}} \end{bmatrix} + \begin{bmatrix} k_{e1} & 0 \\ 0 & k_{e2} \end{bmatrix} \begin{bmatrix} i_{bat} - \hat{i}_{bat} \\ i_{sc} - \hat{i}_{sc} \end{bmatrix}. \tag{12}$$

According to the backward difference method, (12) is converted into discrete form

$$\frac{\hat{i}_{bat}(k) - \hat{i}_{bat}(k-1)}{T_{sc}} = \frac{1}{L_1}[(-d_{01}V_{\mathrm{dc}}(k-1) - R_1\hat{i}_{bat}(k-1) + V_{bat}(k)] + k_{e1}(i_{bat}(k) - \hat{i}_{bat}(k-1)) \tag{13}$$

$$\frac{\hat{i}_{sc}(k) - \hat{i}_{sc}(k-1)}{T_{sc}} = \frac{1}{L_2}[(-d_{23}V_{\mathrm{dc}}(k-1) - R_2\hat{i}_{sc}(k-1) + V_{sc}(k)] + k_{e2}(i_{sc}(k) - \hat{i}_{sc}(k-1)) \tag{14}$$

where T_{sc} is the sample step.

B. Open-Switch Fault Diagnosis

It can be seen from (12) that, by selecting an appropriate gain coefficient matrix, the estimated value can quickly converge to the actual value when the system runs normally. When the open-circuit fault occurs in the power switch, the mathematical model of the bidirectional dc–dc converter system is changed and does not match the model of the observer. Hence, the residual of state quantity between the state observer and the actual system

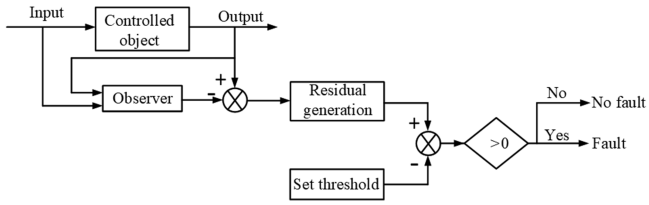

Fig. 4. Fault detection principle.

will diverge rapidly in a short time, and the open-switch fault detection and location are achieved through the residuals of battery current and supercapacitor current.

1) Residual Signal Preprocessing: First, to enhance the robustness of the proposed fault diagnosis method, the residual function $J_r(t)$ based on the moving average filter is determined

$$\begin{cases} J_r(t) = \frac{1}{w}\int_{t-w}^{t} e(\tau)d(\tau) \\ e = x - \hat{x} \end{cases} \tag{15}$$

where e is the state residual between the actual system and the observer, and w is the size of the sliding window.

The residual change greatly after the fault occurs and is far greater than the residual under healthy condition, hence, considering the case that the parameter uncertainty will increase the residual, 1.5 times of the maximum residual during healthy operation is taken as the fault detection threshold

$$J_{th} = 1.5\max\left(|J_r(t)|\right) \tag{16}$$

where J_{th} is the threshold for fault detection.

2) Fault Detection: The open-switch fault of two bidirectional dc–dc converters in HESS is detected when the absolute value of the residual function of the battery current or supercapacitor current exceeds the threshold value. The fault detection principle is shown in Fig. 4.

In addition, the large residuals caused by a sudden change in motor operating point may exceed the threshold and cause false detections. However, the current will drop sharply to close to 0 after the open-circuit fault occurs in power switch, which will contradict the fact that the current is obviously larger than 0 under a sudden change in motor operating point. Hence, the condition that the current is close to 0 can be used to reduce the possibility of false detection caused by the sudden change in motor operating point. Hence, the open-switch fault can be detected based on the following logic:

$$\mathrm{Flag} = \begin{cases} 1 & \begin{array}{c} |J_{i_{bat}}(t)| \geq J_{th}^{i_{bat}} \,\&\, |i_{bat}| \approx 0 \\ \text{or} \\ |J_{i_{sc}}(t)| \geq J_{th}^{i_{sc}} \,\&\, |i_{sc}| \approx 0 \end{array} \\ 0 & \text{otherwise} \end{cases} \tag{17}$$

where $|J_{i_{bat}}(t)|$and $|J_{i_{sc}}(t)|$ are the absolute value of the residual function of the battery current and supercapacitor current, respectively,$J_{th}^{i_{bat}}$ and $J_{th}^{i_{sc}}$ are the thresholds, Flag is the fault detection flag.

3) Fault Location: During the operation process of the electric vehicle, the battery and supercapacitor work in a state of

charging and discharging. The discharging tube and the charging tube can only work alone and cannot work at the same time. Therefore, the situation that the charging tube and the discharging tube fail at the same time does not exist. Moreover, it is rare for the discharging tube or charging tube on the battery side and the supercapacitor side to fail at the same time. Hence, this article mainly focuses on the fault location of a single power tube, and the fault location of the discharging tube and the charging tube is discussed as follow.

a) Discharging tube S_0 *and* S_2*:* First, supposing that the open-circuit fault occurs in the discharging power tube S_0, whether it is in the discharging state or it is changed from the charging state to the discharging state, according to (1), $k = 1$ and (6) is changed into

$$d_{01} = 1 - d_0. \tag{18}$$

After the open-switch fault occurrence, the actual current will decrease rapidly and the reference current cannot be tracked, d_0 will be suddenly changed from 0 to 1. Hence, it has

$$d_{01} V_{\text{dc}} = 0. \tag{19}$$

According to Fig. 1 and Kirchhoff's voltage law, it can be obtained that the battery voltage is larger than the voltage across the resistance R_1, where the resistance R_1 is the circuit wire resistance and it is very small. Hence, it has

$$V_{bat} >> R_1 \hat{i}_{bat}. \tag{20}$$

After the open-switch fault occurrence, the actual current will be not suddenly changed due to the inductance effect. In addition, the inductance L_1 is small, hence, as long as the feedback coefficient k_{e1} is selected properly, the following condition is satisfied:

$$\left| \frac{V_{bat} - R_1 \hat{i}_{bat}}{L_1} \right| \approx \frac{V_{bat}}{L_1} > \left| k_{e1} \left(i_{bat} - \hat{i}_{bat} \right) \right|. \tag{21}$$

By substituting (18)–(21) into (13), after open-circuit fault occurs in the discharging power tube S_0, it has

$$\frac{\hat{i}_{bat}(k) - \hat{i}_{bat}(k-1)}{T_{sc}} > 0. \tag{22}$$

Since two bidirectional dc–dc converters are connected in parallel on the dc bus, the open-circuit fault of the power tube on the battery side will definitely affect the working conditions of the supercapacitor side, which may cause the increase of the supercapacitor current residual or even exceeds the threshold. However, when the feedback coefficients on both sides are set to be near, the change of the current residual on the supercapacitor side must not exceed that on the battery side. Hence, set $k_{e1} = k_{e2}$, it can be obtained as

$$\begin{cases} \frac{\hat{i}_{bat}(k) - \hat{i}_{bat}(k-1)}{T_{sc}} > \frac{\hat{i}_{sc}(k) - \hat{i}_{sc}(k-1)}{T_{sc}} \\ \left| i_{bat} - \hat{i}_{bat} \right| > \left| i_{sc} - \hat{i}_{sc} \right|. \end{cases} \tag{23}$$

From the abovementioned analysis, it can be seen that, after open-circuit fault occurs in the discharging tube S_0, the estimated battery current $\hat{i}_{bat}$will rise rapidly, and the current residual $i_{bat} - \hat{i}_{bat}$ will be smaller than 0, and the absolute value of the battery current residual will be larger than that of the supercapacitor current residual. Because the open-switch fault occurs, the battery current i_{bat} will be rapidly changed from positive to close to 0, and $\hat{i}_{bat}$ is larger than 0.

In addition, since the bidirectional dc–dc converters on the battery side and the supercapacitor side have the same structure and are symmetrical, the abovementioned conclusion is also valid when the open-circuit fault occurs in the discharging tube S_2.

b) Charging tube S_1 *and* S_3*:* Supposing that the charging power tube S_1 has open-circuit fault, whether it is in the charging state or it is changed from the discharging state to the charging state, according to (1), $k = 1$ and (6) is changed into

$$d_{01} = d_1. \tag{24}$$

After the open-switch fault occurrence, the actual current will decrease rapidly and the reference current cannot be tracked, d_1 will be suddenly changed from 0 to 1. Hence, it has

$$d_{01} V_{\text{dc}} = V_{\text{dc}}. \tag{25}$$

Similarly, the battery voltage is larger than the resistance voltage across its loop. This resistance is the loop wire resistance R_1 and it is very small. Hence, it has

$$V_{bat} >> R_1 \hat{i}_{bat}. \tag{26}$$

Since the dc bus voltage is obtained by boosting the battery and the supercapacitor, the dc bus voltage is larger than the battery voltage. Hence, it has

$$V_{dc} > V_{bat}. \tag{27}$$

After an open-switch fault occurs, the actual current will be not suddenly changed due to the inductance effect. Moreover, the inductance L_1 is small, so as long as the feedback coefficient k_{e1} is selected properly, the following condition is satisfied:

$$\left| \frac{V_{bat} - R_1 \hat{i}_{bat} - V_{\text{dc}}}{L_1} \right| \approx \left| \frac{V_{bat} - V_{\text{dc}}}{L_1} \right| > \left| k_{e1} \left(i_{bat} - \hat{i}_{bat} \right) \right|. \tag{28}$$

By substituting (24)–(28) into (13), after the open-circuit fault occurs in the charging power tube S_1, it has

$$\frac{\hat{i}_{bat}(k) - \hat{i}_{bat}(k-1)}{T_{sc}} < 0. \tag{29}$$

Similarly, set $k_{e1} = k_{e2}$, it has

$$\begin{cases} \left| \frac{\hat{i}_{bat}(k) - \hat{i}_{bat}(k-1)}{T_{sc}} \right| > \left| \frac{\hat{i}_{sc}(k) - \hat{i}_{sc}(k-1)}{T_{sc}} \right| \\ \left| i_{bat} - \hat{i}_{bat} \right| > \left| i_{sc} - \hat{i}_{sc} \right| \end{cases}. \tag{30}$$

According to the abovementioned analysis, it is seen that, after open-circuit fault occurs in the charging tube S_1, the estimated battery current $\hat{i}_{bat}$ will drop rapidly, and the current residual $i_{bat} - \hat{i}_{bat}$ will be larger than 0, and the absolute value of the battery current residual will be larger than that of the supercapacitor current residual. As the open-switch fault occurs, the

TABLE I
SUMMARY OF FLAGS UNDER HEALTHY AND FAULT CONDITIONS

State	*Flag*	$Flag_0$	$Flag_1$	$Flag_2$	$Flag_3$
Healthy	0	0	0	0	0
S_0 open fault	1	1	0	0	0
S_1 open fault	1	0	1	0	0
S_2 open fault	1	0	0	1	0
S_3 open fault	1	0	0	0	1

battery current i_{bat} will be rapidly changed from negative to close to 0, and $\hat{i}_{bat}$ is smaller than 0. Similarly, the abovementioned conclusion is also suitable for open-circuit fault in the charging power tube S_3.

Hence, the open-switch fault can be located based on the following logic:

$$\text{Flag}_0 = \begin{cases} 1 & \hat{i}_{bat} > 0 \& |J_{i_{bat}}| > |J_{i_{sc}}| \\ 0 & \text{otherwise} \end{cases} \tag{31}$$

$$\text{Flag}_1 = \begin{cases} 1 & \hat{i}_{bat} < 0 \& |J_{i_{bat}}| > |J_{i_{sc}}| \\ 0 & \text{otherwise} \end{cases} \tag{32}$$

$$\text{Flag}_2 = \begin{cases} 1 & \hat{i}_{sc} > 0 \& |J_{i_{bat}}| < |J_{i_{sc}}| \\ 0 & \text{otherwise} \end{cases} \tag{33}$$

$$\text{Flag}_3 = \begin{cases} 1 & \hat{i}_{sc} < 0 \& |J_{i_{bat}}| < |J_{i_{sc}}| \\ 0 & \text{otherwise} \end{cases} \tag{34}$$

where Flag_0, Flag_1, Flag_2, and Flag_3 are power tube S_0, S_1, S_2, and S_3 open-fault location flags, respectively.

In summary, the open-switch fault diagnosis process is described as follows.

Step 1: The fault detection is achieved by the absolute value of the battery/supercapacitor current residual and the battery/supercapacitor current, as expressed in (17).

Step 2: The fault side location is obtained by judging, which side has the larger absolute value of the current residual.

Step 3: The faulty power tube location is achieved by the estimated current. If the value of the estimated current is larger than 0, it is indicated that the discharging power tube has an open-circuit fault. If the value of the estimated current is smaller than 0, the charging power tube has an open-circuit fault.

In addition, Table I summarizes fault detection and location flags, and fault diagnosis flowchart is shown in Fig. 5.

IV. SIMULATION VALIDATION

To validate the proposed open-switch fault diagnosis method, the simulation is carried out in MATLAB/Simulink environment. The specific parameters of two bidirectional dc–dc converters in HESS are listed in Table II.

A. Open-Circuit Fault in Discharging Tube S_0 on Battery Side

Fig. 6 shows the simulation waveforms for the open-circuit fault in S_0 at the moment $t = 2.4$ s. It is seen that, under healthy condition, the estimated current can track the actual value, and

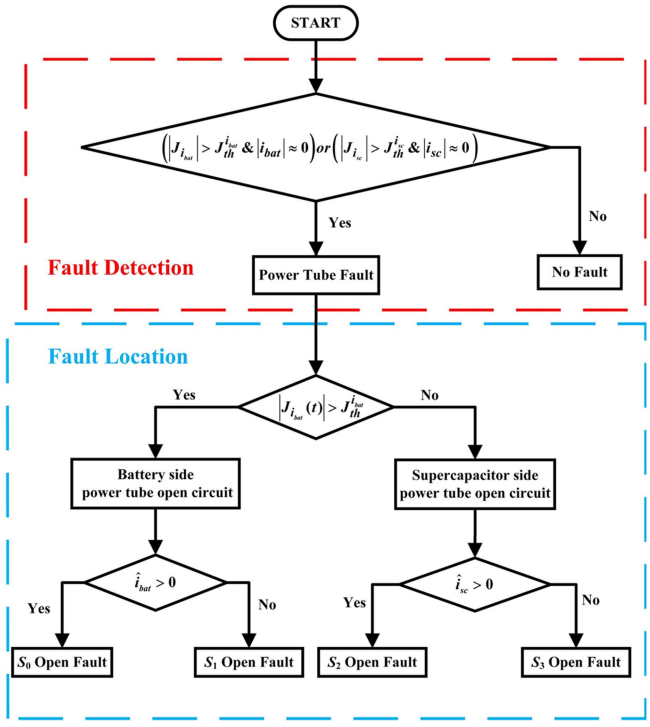

Fig. 5. Fault diagnosis flowchart.

TABLE II
SPECIFIC PARAMETERS OF TWO BIDIRECTIONAL DC–DC CONVERTERS IN HESS

Battery Voltage (V)	36	C_{dc} (mF)	66
Supercapacitor Voltage (V)	36	k_{e1}	500
DC Bus Voltage (V)	60	k_{e2}	500
L (mH)	10	Sample Frequency (kHz)	50
R (Ω)	0.3	Switching Frequency (kHz)	10
$J_{th}^{i_{bat}}$ (A)	0.3	$J_{th}^{i_{sc}}$ (A)	0.8

the residual is small. The fault detection and location flags (Flag, Flag_0, Flag_1, Flag_2, Flag_3) are all equal to zero. As the open-switch fault occurs, the battery current drops rapidly to close to 0, the estimated battery current rises rapidly above 0, and the absolute value of the battery current residual exceeds the threshold. The absolute value of the battery current residual is larger than that of the supercapacitor current residual. Moreover, both the flags Flag and Flag_0 are changed and are equal to 1 at the instant $t = 2.4005$ s, and the remaining flags Flag_1, Flag_2, and Flag_3 are not changed. Hence, the simulation results show that, by the fault detection and location flags Flag and Flag_{0123}, the open-switch fault can be effectively detected and located 0.0005 s after the fault occurrence.

B. Open-Circuit Fault in Charging Tube S_1 on Battery Side

Fig. 7 shows the simulation waveforms for the open-circuit fault in S_1 at the moment $t = 2.7$ s. Under healthy condition, the estimated currents can track the actual currents, and the current residuals are small. The fault detection and location flags

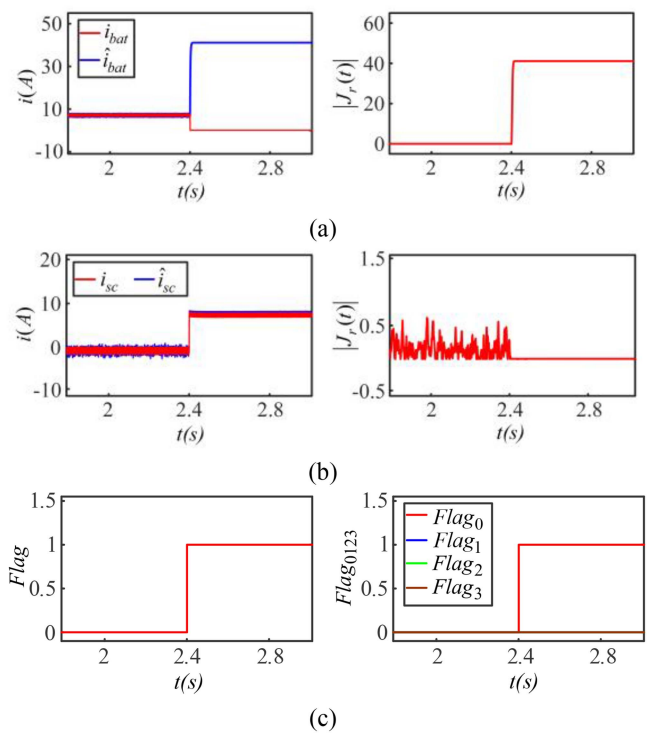

Fig. 6. Simulation waveforms for open-circuit fault in S_0. (a) Actual and estimated valves of the battery current (left) and the absolute value of residual (right). (b) Actual and estimated valves of the supercapacitor current (left) and the absolute value of residual (right). (c) Flags of fault detection (left) and fault location (right).

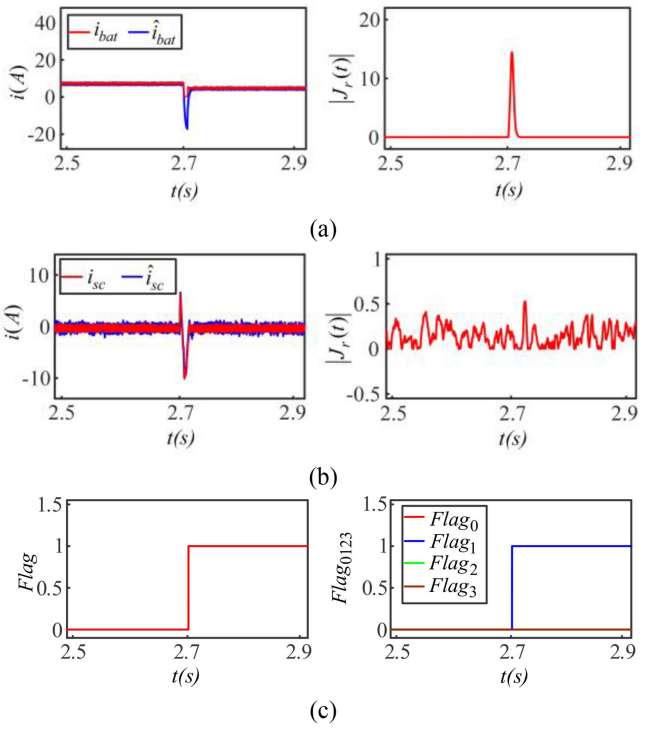

Fig. 7. Simulation waveforms for open-circuit fault in S_1. (a) Actual and estimated valves of the battery current (left) and the absolute value of residual (right). (b) Actual and estimated valves of the supercapacitor current (left) and the absolute value of residual (right). (c) Flags of fault detection (left) and fault location (right).

are all equal to 0. As the open-switch fault occurs, the battery current drops rapidly to close to 0, the estimated battery current drops rapidly below 0, and the absolute value of the battery current residual exceeds the threshold. The working state of the supercapacitor is less affected by the open-switch fault, and the supercapacitor current residual has slight change. The absolute value of the battery current residual is larger than that of the supercapacitor current residual. Moreover, both the flags Flag and Flag_1 are changed and are equal to 1 at the instant $t = 2.7005$ s, and the remaining flags are not changed. Hence, the simulation results show that, by the fault detection and location flags, the open-switch fault can be detected and located 0.0005 s after the fault occurrence.

In addition, the simulation waveforms of open-circuit fault in the discharging tube S_2 and charging tube S_3 on the supercapacitor side are presented in Figs. 8 and 9, respectively. The simulation results show that the open-switch fault can be also detected and located by the fault detection and location flags as the fault occurs in the discharging tube S_2 and charging tube S_3 on the supercapacitor side.

C. Effect of Parameter Uncertainty

The observer is based on the mathematical model of the system and requires precise model parameters, such as L and R. As is known, the parameters are affected by the temperature, operating

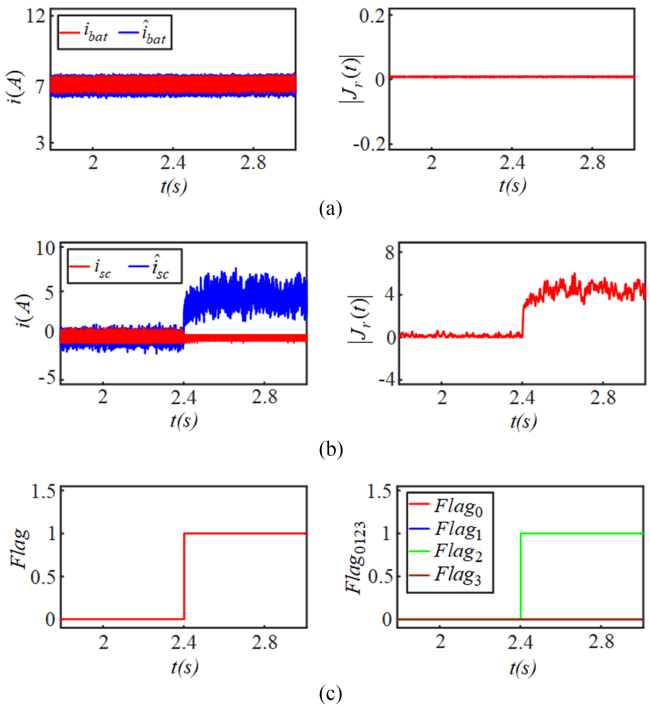

Fig. 8. Simulation waveforms for open-circuit fault in S_2. (a) Actual and estimated valves of the battery current (left) and the absolute value of residual (right). (b) Actual and estimated valves of the supercapacitor current (left) and the absolute value of residual (right). (c) Flags of fault detection (left) and fault location (right).

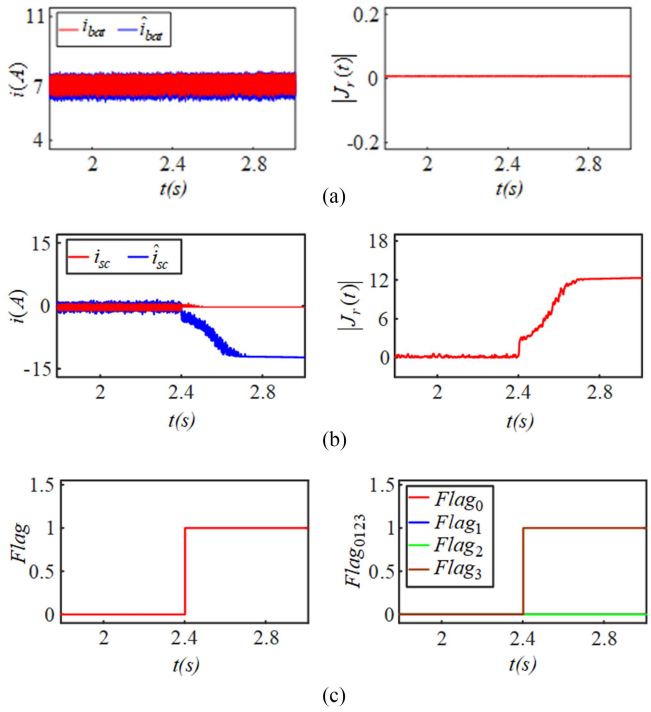

Fig. 9. Simulation waveforms for open-circuit fault in S_3. (a) Actual and estimated valves of the battery current (left) and the absolute value of residual (right). (b) Actual and estimated valves of the supercapacitor current (left) and the absolute value of residual (right). (c) Flags of fault detection (left) and fault location (right).

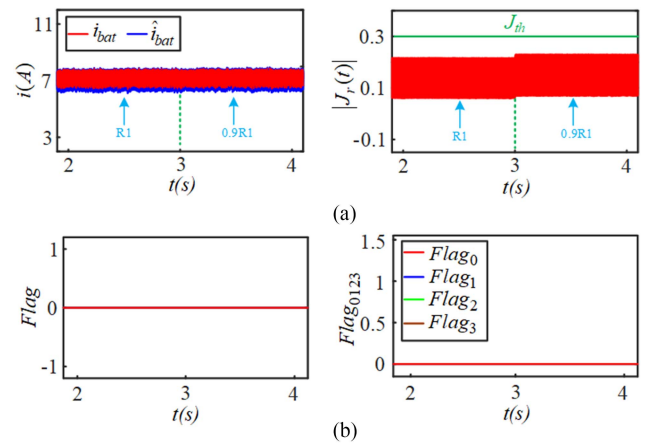

Fig. 10. Simulation result under the condition that the value of R_1 varies by -10% at the instant $t = 3$ s. (a) Actual and estimated valves of the battery current (left) and the absolute value of residual (right). (b) Flags of fault detection (left) and fault location (right).

conditions, and so on. Hence, to investigate the effect of the parametric uncertainty on the proposed method, the simulation are performed under different situations.

Supposing the value of L_1 and R_1 varies. Figs. 10 and 11 show the simulation results under the condition that the value of R_1 and L_1 varies by -10% at the instant $t = 3$ s. As seen from Figs. 10 and 11, when the parameter changes are not obvious, the residual will become larger, but it does not exceed the set

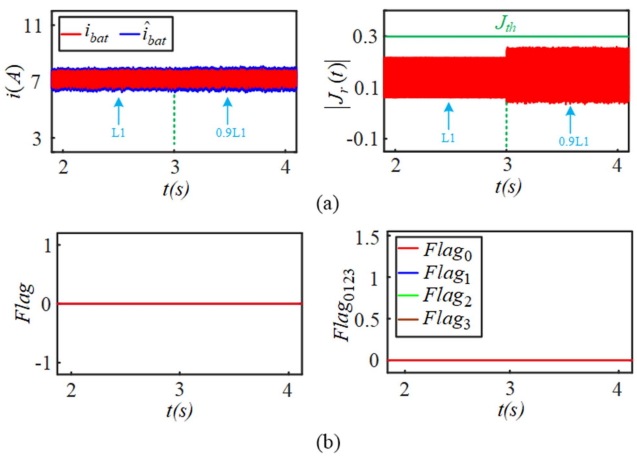

Fig. 11. Simulation result under the condition that the value of L_1 varies by -10% at the instant $t = 3$ s. (a) Actual and estimated valves of the battery current (left) and the absolute value of residual (right). (b) Flags of fault detection (left) and fault location (right).

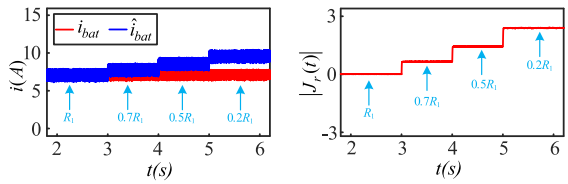

Fig. 12. Simulation result under the condition that the value of R_1 varies by -30%, -50%, and -80%.

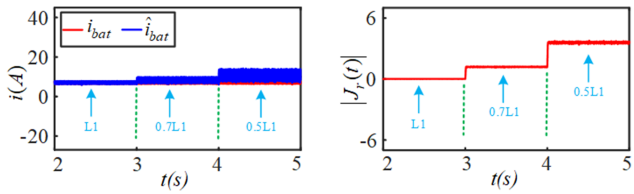

Fig. 13. Simulation result under the condition that the value of L_1 varies by -30% and -50%.

threshold of 0.3. Therefore, the fault detection and fault location flags are not triggered.

In addition, to fully understand the impact of parameter changes, it is necessary to conduct the research on the case that the parameter changes are obvious. Supposing that the value of L_1 and R_1 varies by -30%, -50%, and -80%. As seen from Figs. 12 and 13, when the parameters change significantly, the residuals exceed the threshold value of 0.3, leading to false diagnosis. However, the parameter changes are usually small [32], [33], and the proposed method can still achieve the reliable open-circuit fault diagnosis.

D. Short-Circuit Fault

The short-circuit fault in the battery side discharge tube S_0 is taken as an example, and the simulation results are presented in Fig. 14. It can be seen that, after the discharge tube is short-circuited at the moment $t = 2.4$ s, the current residual increases sharply and quickly exceeds the threshold value, and

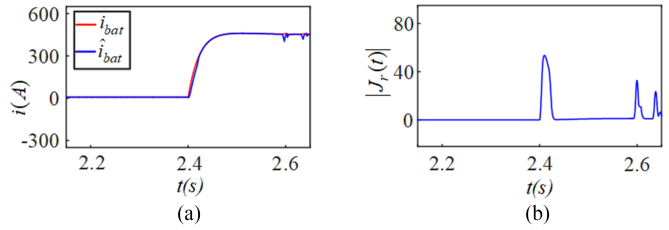

Fig. 14. Simulation results for short-circuit fault in S_0. (a) Actual and estimated valves of the battery current. (b) Absolute value of residual.

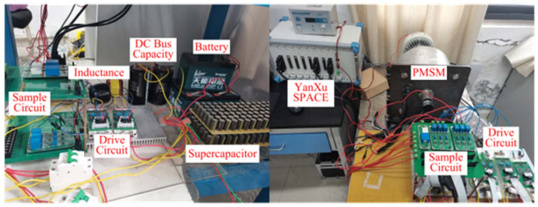

Fig. 15. Experimental platform.

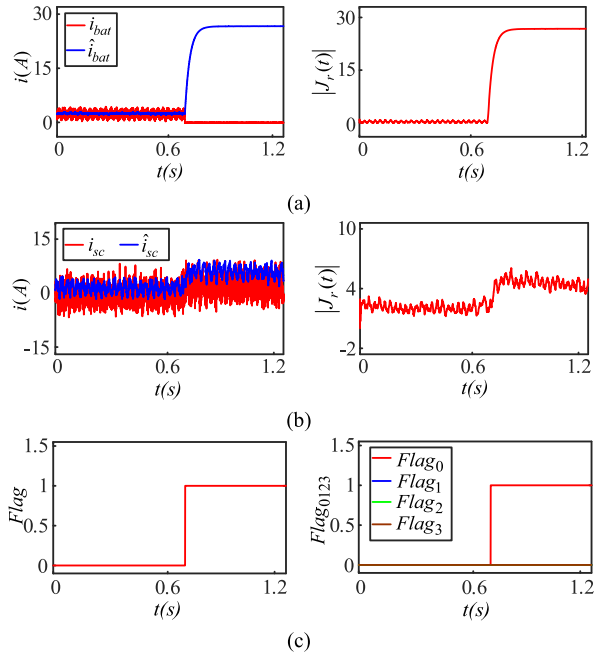

Fig. 16. Experimental waveforms for the open-circuit fault in S_0. (a) Actual and estimated valves of the battery current (left) and the absolute value of residual (right). (b) Actual and estimated valves of the supercapacitor current (left) and the absolute value of residual (right). (c) Flags of fault detection (left) and fault location (right).

the estimated value is much larger than 0. It is shown that the rapid fault diagnosis can be also carried out by the proposed method. However, after the short-circuit fault occurs, the current increased dramatically far beyond the maximum allowable current of the system. Hence, the short-circuit fault is very dangerous, and the short-circuit fault is usually converted into open-circuit fault by adding fast fuses in the converter [4]. Hence, only the power tube open circuit fault diagnosis is studied in this article.

V. Experimental Verification

A. Experimental Platform

To further verify the proposed fault diagnosis method, an experimental platform of the hybrid energy source fed PMSM system is built, as shown in Fig. 15, which mainly includes batteries, supercapacitors, a PMSM, two inductances, two electrolytic capacitors, two sampling circuits, and a YX Space controller. Together with the MATLAB/Simulink and YX Space controller, the YX Space controller provides real time control and monitoring of the hybrid energy source fed PMSM system. In addition, the open-circuit fault in power tube is simulated by setting PWM signal to 0. In addition, the parameters ($J_{th}^{i_{bat}}$, $J_{th}^{i_{sc}}$, k_{e1}, and k_{e2}) of the proposed fault diagnosis method are chosen to be 1.5, 4, 500, and 500 in the experimental tests, respectively.

B. Experimental Results

1) Open-Circuit Fault of the Discharging Tube S_0 on the Battery Side: Fig. 16 shows the experimental waveforms for the open-circuit fault in S_0 about t = 0.7 s. It is seen that the experimental results are similar with the simulation results in Fig. 6. Under healthy condition, the estimated currents are close to the actual currents and the current residuals are small. The fault detection and location flags (Flag, Flag_0, Flag_1, Flag_2, Flag_3) are all equal to zero. As the open-switch fault occurs, the battery current drops rapidly to close to 0, the estimated battery current rises rapidly above 0, and the absolute value of the battery current residual exceeds the threshold. The absolute value of the battery current residual is larger than that of the supercapacitor current residual. The flags Flag and Flag_0 are changed from 0 to 1 after the fault, and the remaining flags Flag_1, Flag_2, and Flag_3 are kept 0. Hence, the experimental results indicate that the open-switch fault can be detected and located after the fault occurrence by the fault detection and location flags Flag and Flag_{0123}.

2) Open-Circuit Fault of the Charging Tube S_1 on the Battery Side: Fig. 17 shows the experimental waveforms for the open-circuit fault in S_1 about t = 2.6 s. It is seen that the experimental results are also similar with the simulation results in Fig. 7. Under healthy condition, the estimated currents can track the actual currents, and the current residuals are small. The fault detection and location flags are all equal to 0. Under fault condition, the battery current drops rapidly to close to 0, the estimated battery current drops rapidly below 0, and the absolute value of the battery current residual exceeds the threshold. The absolute value of the battery current residual is larger than that of the supercapacitor current residual. The flags Flag and Flag_1 are both changed from 0 to 1 after the fault, and the remaining flags are kept 0. The experimental results show that, by the fault detection and location flags, the open-switch fault can be effectively detected and located.

Moreover, the experimental waveforms of open-circuit fault in the discharging tube S_2 and charging tube S_3 on the

TABLE III
COMPARISON OF OPEN-CIRCUIT FAULT DIAGNOSIS METHODS OF DC–DC CONVERTERS

Fault diagnosis method	Cost	Robustness	Adaptability	Detection time	Fault location
Inductor current [5-9]	Low	Low	Weak	2 switching periods	No
Inductor/diode voltage [10-13][16]	High	Low	Weak	1 switching periods	No
Magnetic near-field signal [14]	High	High	Strong	No specific time	Yes
Buck or Boost observer [22-23]	Low	High	Weak	No specific time	Yes
Proposed method	Low	High	Strong	5 switching periods	Yes

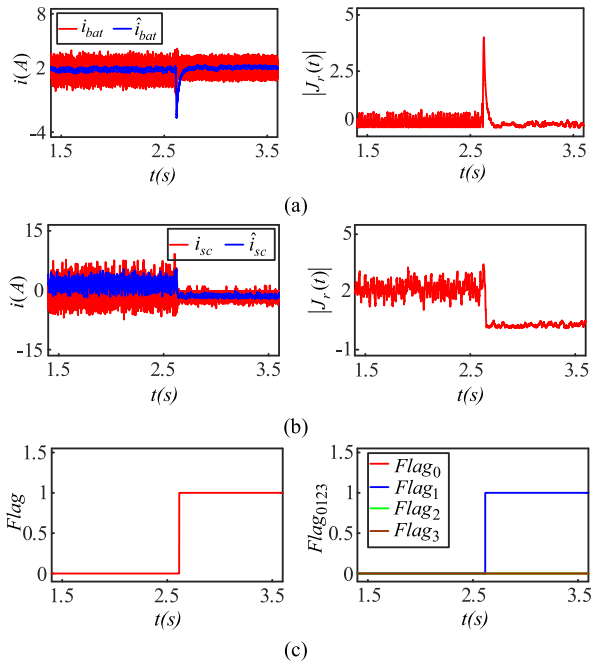

Fig. 17. Experimental waveforms for the open-circuit fault in S_1. (a) Actual and estimated valves of the battery current (left) and the absolute value of residual (right). (b) Actual and estimated valves of the supercapacitor current (left) and the absolute value of residual (right). (c) Flags of fault detection (left) and fault location (right).

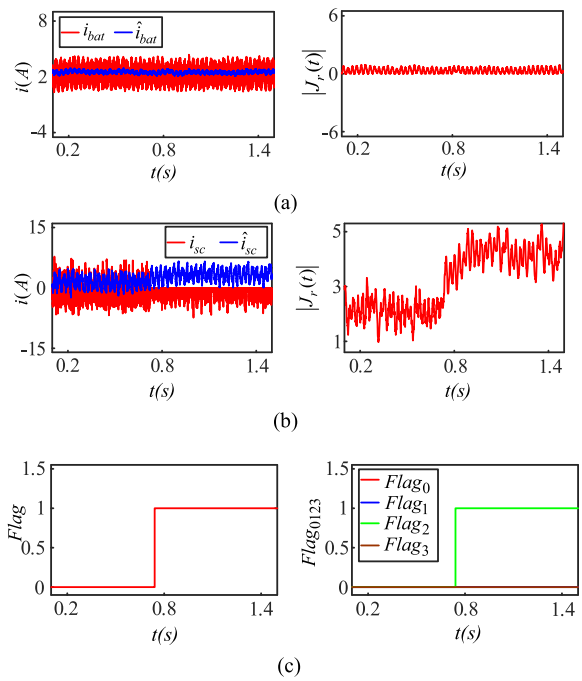

Fig. 18. Experimental waveforms for the open-circuit fault in S_2. (a) Actual and estimated valves of the battery current (left) and the absolute value of residual (right). (b) Actual and observed valves of the supercapacitor current (left) and the absolute value of residual (right). (c) Flags of fault detection (left) and fault location (right).

supercapacitor side are presented in Figs. 18 and 19, respectively. The experimental results indicate that, by fault detection and location flags, the open-switch fault can be also detected and located as the fault occurs in the discharging tube S_2 and charging tube S_3 on the supercapacitor side.

3) Effect of Parameter Uncertainty: In order to further verify the influence of parameter uncertainty on the diagnostic method, the experimental study is performed under different situations, as presented in Figs. 20 and 21. The results show that, when the parameter changes are not obvious, false diagnosis are not triggered; for large parameter changes, the residuals exceed the threshold, leading to false diagnosis, being in agreement with simulation results.

4) Transient Process: Fig. 22 shows the experimental results with the load switching from full load nonload. It is seen that, when the load changes suddenly, the actual currents of the battery and supercapacitor are greater than 0 and does not meet the condition that the absolute values of the currents are close to 0, and the fault detection will not be triggered.

C. Comparisons

To show the limitations and strengths of the proposed method and previous methods, a few important indicators are chosen to study the limitations and strengths of the proposed method and previous methods, such as cost (additional hardware and sensors), robustness (load disturbances), adaptability, detection time, and fault location. The comparison results are presented in Table III.

The fault diagnosis method based on inductive current and inductive voltage has poor robustness when detecting the critical value of duty or high switching frequency [5]. In addition, the signals of actual current and voltage are greatly affected by the control strategy, which fluctuates and contains the measurement

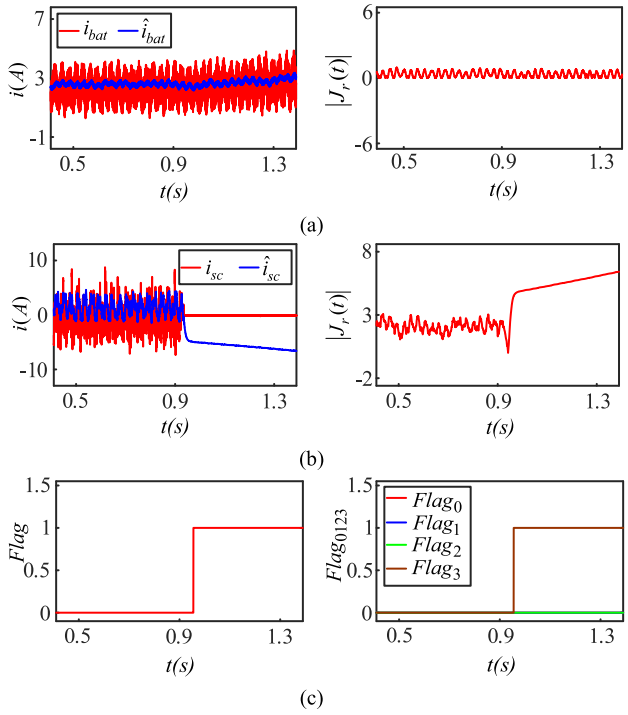

Fig. 19. Experimental waveforms for the open-circuit fault in S_3. (a) Actual and estimated valves of the battery current (left) and the absolute value of residual (right). (b) Actual and estimated valves of the supercapacitor current (left) and the absolute value of residual (right). (c) Flags of fault detection (left) and fault location (right).

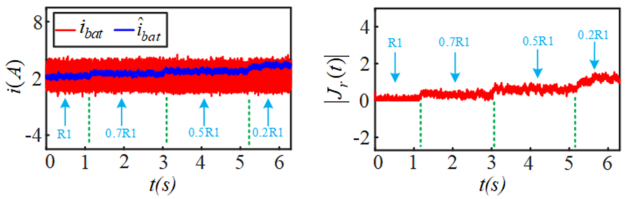

Fig. 20. Experimental result under the condition that the value of R_1 varies by −30%, −50%, and −80%.

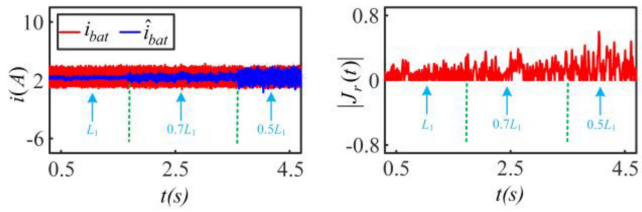

Fig. 21. Experimental results under the condition that the value of L_1 varies by −30% and −50%.

noise signal. Therefore, the inductive current slope and voltage fluctuate greatly, and it is difficult to find the appropriate fault diagnosis threshold, so the robustness is poor. In addition, this method is only suitable for specific converters, and the characteristics of current and voltage signals in different converters are quite different, so it is difficult to find common fault characteristics, and the adaptability is poor. However, due to

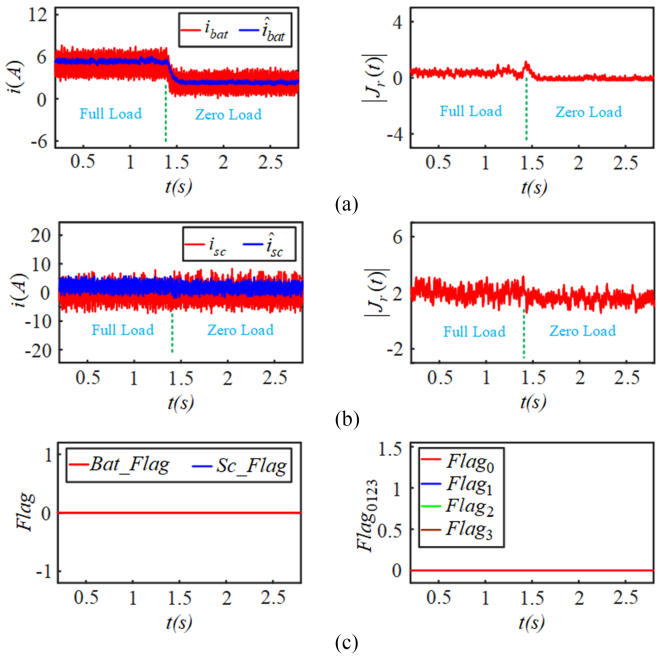

Fig. 22. Experimental results of the load switching from full load to zero. (a) Actual and estimated valves of the battery current (left) and the absolute value of residual (right) from full load to zero. (b) Actual and estimated valves of the Supercapacitor current (left) and the absolute value of residual (right) from full load to zero. (c) Flags of fault detection (left) and fault location (right).

the small amount of calculation, the fault can be usually detected no more than two switching periods.

The fault diagnosis method based on magnetic near-field signal can capture magnetic fields from different sources, and the measurement waveform contains rich diagnostic information, so it has strong robustness [12]. In addition, when the dc–dc converter works in the switching mode, it will radiate strong electromagnetic noise. Because the electromagnetic noise is caused by the change of current and voltage, it carries a wealth of useful information [34], [35]. Hence, this method can be extended and applied to other types of converters with strong adaptability. But the calculation is complicated and the detection time is long.

The fault diagnosis method based on independent buck/boost observer contains all the information of state quantities. Moreover, the algorithm of the observer has high precision, strong stability and low phase lag, so it has strong robustness. At the same time, as long as the mathematical model of the converter is derived, it can be applied to various types of converters, so it has strong adaptability. However, as the observer in multiple modes is established, the calculation is large and the detection time is long. On the contrary, the proposed method derives the global mathematical model of the converter, so that only one state observer is built to observe the state quantities in all modes, and the calculation is relatively small and the detection time is shorter.

In summary, the detection time of the proposed method is not the least among the several methods. However, it is relatively best on basis of comprehensive consideration of cost, robustness,

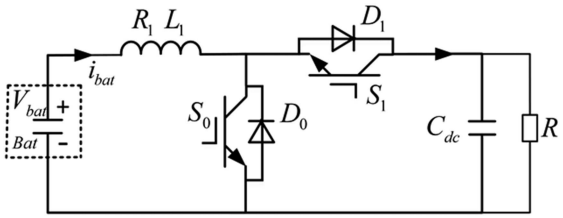

Fig. 23. Equivalent topology in battery discharging state.

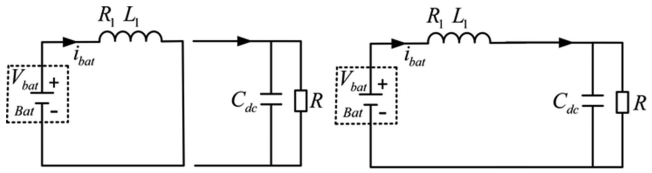

Fig. 24. Equivalent circuit for S_0 ON (left) and OFF (right) state in the discharging state.

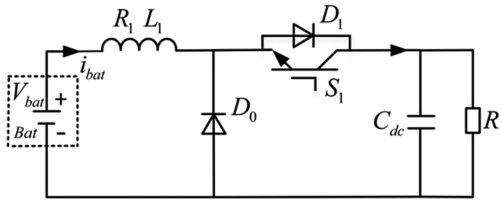

Fig. 25. Equivalent topology in battery charging state.

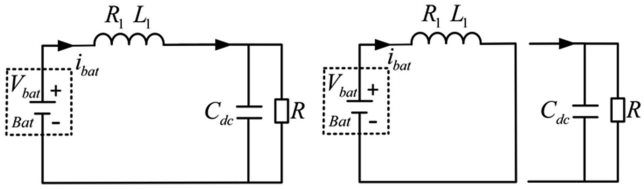

Fig. 26. Equivalent circuit for S_1 ON (left) and OFF (right) state in the charging state.

adaptability, and detection time, indicating that the proposed fault diagnosis has effective performance.

VI. Conclusion

This article proposes a global state observer-based open-switch fault diagnosis method for two bidirectional dc–dc converters in HESS. In this method, the open-switch fault is detected by the absolute value of the battery/supercapacitor current residual and the battery/supercapacitor current. The fault side location is determined by judging, which side has the larger absolute value of the current residual. The fault location is achieved by the estimated current. A hybrid energy source fed PMSM system is built for simulation and experimental verification. Both the results show that the proposed fault diagnosis method can effectively achieve the open-switch fault detection and location.

In addition, it is noted that the large parameter variations may lead to the false diagnosis. The future study will focus on how to remove the influence of parameter changes on the open-switch fault diagnosis method, improving the reliability of fault diagnosis.

Appendix

The battery discharging state indicates that the bidirectional dc–dc converter works at the boost mode. The topology is shown in Fig. 23. At this time, S_1 is always in an OFF state, which is only equivalent to a freewheeling diode. According to the state of power tube S_0, the circuit works in two states. When S_0 is turned ON, the inductor L stores the energy, and the capacitor $C_{\rm dc}$ releases energy to the equivalent load R; when S_0 is turned OFF, the battery and the inductor L simultaneously discharging, and the equivalent circuit is shown in Fig. 24.

The battery current i_{bat} is defined as the state variable of the model. According to Kirchhoff's law KVL, the state equation in the discharging state can be expressed as

$$\frac{di_{bat}}{dt} = -(1-v_0)\frac{V_{dc}}{L_1} - \frac{R_1}{L_1}i_{bat} + \frac{V_{bat}}{L_1}. \tag{A1}$$

Similarly, the state equation of the supercapacitor current i_{sc} in the discharging state can be obtained as

$$\frac{di_{sc}}{dt} = -(1-v_2)\frac{V_{\rm dc}}{L_2} - \frac{R_2}{L_2}i_{sc} + \frac{V_{sc}}{L_2}. \tag{A2}$$

A state equation of the battery current in the charging state is established by a similar method. The equivalent circuit in the charging state is shown in Fig. 25, and the equivalent circuit in the ON and OFF states of the power tube S_1 is shown in Fig. 26.

The state equation in the charging state can be expressed as

$$\frac{di_{bat}}{dt} = -v_1\frac{V_{\rm dc}}{L_1} - \frac{R_1}{L_1}i_{bat} + \frac{V_{bat}}{L_1}. \tag{A3}$$

Similarly, the state equation of the supercapacitor current in the charging state can be obtained as

$$\frac{di_{sc}}{dt} = -v_3\frac{V_{\rm dc}}{L_2} - \frac{R_2}{L_2}i_{sc} + \frac{V_{sc}}{L_2}. \tag{A4}$$

References

[1] C. C. Zhang, J. Dong, and J. Liu, "A control strategy for battery-ultracapacitor hybrid energy storage system," *Trans. China Electrotechnical Soc.*, vol. 29, no. 4, pp. 334–340, 2014.

[2] "Report of large motor reliability survey of industrial and commercial installations, part I," *IEEE Trans. Ind. Appl.*, vol. IA-21, no. 4, pp. 853–864, Jul. 1985.

[3] S. Yang, A. Bryant, P. Mawby, D. Xiang, L. Ran, and P. Tavner, "An industry-based survey of reliability in power electronic converters," *IEEE Trans. Ind. Appl.*, vol. 47, no. 3, pp. 1441–1451, May/Jun. 2011.

[4] C. Cecati, A. O. Di Tommaso, F. Genduso, R. Miceli, and G. R. Galluzzo, "Comprehensive modeling and experimental testing of fault detection and management of a nonredundant fault-tolerant VSI," *IEEE Trans. Ind. Electron.*, vol. 62, no. 6, pp. 3945–3954, Jun. 2015.

[5] E. Jamshidpour, P. Poure, E. Gholipour, and S. Saadate, "Single-switch DC-DC converter with fault-tolerant capability under open- and short-circuit switch failures," *IEEE Trans. Power Electron.*, vol. 30, no. 5, pp. 2703–2712, May 2015.

[6] E. Jamshidpour, P. Poure, and S. Saadate, "Photovoltaic systems reliability improvement by real-time FPGA-based switch failure diagnosis and fault-tolerant DC-DC converter," *IEEE Trans. Ind. Electron.*, vol. 62, no. 11, pp. 7247–7255, Nov. 2015.

[7] M. Shahbazi, E. Jamshidpour, P. Poure, S. Saadate, and M. R. Zolghadri, "Open- and short-circuit switch fault diagnosis for nonisolated DC-DC converters using field programmable gate array," *IEEE Trans. Ind. Electron.*, vol. 60, no. 9, pp. 4136–4146, Sep. 2013.
[8] E. Farjah, H. Givi, and T. Ghanbari, "Application of an efficient Rogowski coil sensor for switch fault diagnosis and capacitor ESR monitoring in non-isolated single-switch DC-DC converters," *IEEE Trans. Power Electron.*, vol. 32, no. 2, pp. 1442–1456, Feb. 2017.
[9] S. Jagtap and D. More, "Switch open-circuit fault diagnosis and fault-tolerant control strategy for DC-DC converters," in *Proc. Int. Conf. Commun. Signal Process.*, 2020, pp. 1399–1405.
[10] H. K. Cho, S. S. Kwak, and S. H. Lee, "Fault diagnosis algorithm based on switching function for boost converters," *Int. J. Electron.*, vol. 102, no. 7, pp. 1229–1243, 2015.
[11] X. Pei, S. Nie, Y. Chen, and Y. Kang, "Open-circuit fault diagnosis and fault-tolerant strategies for full-bridge DC-DC converters," *IEEE Trans. Power Electron.*, vol. 27, no. 5, pp. 2550–2565, May 2012.
[12] S. Nie, X. Pei, Y. Chen, and Y. Kang, "Fault diagnosis of PWM DC-DC converters based on magnetic component voltages equation," *IEEE Trans. Power Electron.*, vol. 29, no. 9, pp. 4978–4988, Sep. 2014.
[13] H. Wang, X. Pei, Y. Wu, Y. Xiang, and Y. Kang, "Switch fault diagnosis method for series-parallel forward DC-DC converter system," *IEEE Trans. Ind. Electron.*, vol. 66, no. 6, pp. 4684–4695, Jun. 2019.
[14] Y. Chen, X. Pei, S. Nie, and Y. Kang, "Monitoring and diagnosis for the DC-DC converter using the magnetic near field waveform," *IEEE Trans. Ind. Electron.*, vol. 58, no. 5, pp. 1634–1647, May 2011.
[15] A. M. Airabella, L. E. Piris-Botalla, C. A. Falco, G. O. García, and G. G. Oggier, "Semi-conductors faults analysis in dual active bridge DC-DC converter," *Int. Eng. Technol. Power Electron.*, vol. 9, no. 6, pp. 1103–1110, May 2016.
[16] H. Givi, E. Farjah, and T. Ghanbari, "Switch and diode fault diagnosis in non-isolated DC-DC converters using diode voltage signature," *IEEE Trans. Ind. Electron.*, vol. 65, no. 2, pp. 1606–1615, Feb. 2018.
[17] E. Ribeiro, A. J. M. Cardoso, and C. Boccaletti, "Open-circuit fault diagnosis in interleaved DC-DC converters," *IEEE Trans. Power Electron.*, vol. 29, no. 6, pp. 3091–3102, Jun. 2014.
[18] M. W. Ahmad, N. B. Y. Gorla, H. Malik, and S. K. Panda, "A fault diagnosis and postfault reconfiguration scheme for interleaved boost converter in PV-based system," *IEEE Trans. Power Electron.*, vol. 36, no. 4, pp. 3769–3780, Apr. 2021.
[19] K. Bi, Q. An, J. Duan, L. Sun, and K. Gai, "Fast diagnostic method of open circuit fault for modular multilevel DC/DC converter applied in energy storage system," *IEEE Trans. Power Electron.*, vol. 32, no. 5, pp. 3292–3296, May 2017.
[20] H. Wen, J. Li, H. Shi, Y. Hu, and Y. Yang, "Fault diagnosis and tolerant control of dual-active-bridge converter with triple-phase shift control for bidirectional EV charging systems," *IEEE Trans. Transp. Electrific.*, vol. 7, no. 1, pp. 287–303, Mar. 2021.
[21] H. Givi, E. Farjah, and T. Ghanbari, "Switch fault diagnosis and capacitor lifetime monitoring technique for DC-DC converters using a single sensor," *Int. Eng. Technol. Sci., Meas. Technol.*, vol. 10, no. 5, pp. 513–527, Aug. 2016.
[22] Y. Guo, Z. Song, J. Xia, and X. Zhang, "Fault diagnosis and fault-tolerant control for the sensors of DC-DC boost converter," in *Proc. 37th Chin. Control Conf.*, 2018, pp. 7594–7599.
[23] P. Jain et al., "A luenberger observer-based fault detection and identification scheme for photovoltaic DC-DC converters," in *Proc. IECON 43rd Annu. Conf. IEEE Ind. Electron. Soc.*, 2017, pp. 5015–5020.
[24] N. M. Mukhtar and D. D.-C. Lu, "A bidirectional two-switch flyback converter with cross-coupled LCD snubbers for minimizing circulating current," *IEEE Trans. Ind. Electron.*, vol. 66, no. 8, pp. 5948–5957, Aug. 2019.
[25] C. Li et al., "Design and implementation of a bidirectional isolated cuk converter for low-voltage and high-current automotive DC source applications," *IEEE Trans. Veh. Technol.*, vol. 63, no. 6, pp. 2567–2577, Jul. 2014.
[26] S. Li, K. Xiangli, and K. M. Smedley, "A control map for a bidirectional PWM plus phase-shift-modulated push–pull DC–DC converter," *IEEE Trans. Ind. Electron.*, vol. 64, no. 11, pp. 8514–8524, Nov. 2017.
[27] F. Zhang and Y. Yan, "Novel forward–flyback hybrid bidirectional DC–DC converter," *IEEE Trans. Ind. Electron.*, vol. 56, no. 5, pp. 1578–1584, May 2009.
[28] H. Li, L. Zhao, C. Xu, and X. Zheng, "A dual half-bridge phaseshifted converter with wide ZVZCS switching range," *IEEE Trans. Power Electron.*, vol. 33, no. 4, pp. 2976–2985, Apr. 2018.
[29] R. M. Schupbach and J. C. Balda, "Comparing DC-DC converters for power management in hybrid electric vehicles," in *Proc. IEEE Int. Electric Machines Drives Conf.*, 2003, vol. 3, pp. 1369–1374.
[30] E. Ribeiro, A. J. M. Cardoso, and C. Boccaletti, "Modular hybrid storage system for renewable energy standalone power supplies," in *Proc. 39th Annu. Conf. IEEE Ind. Electron. Soc.*, 2013, pp. 1749–1754.
[31] J. G. Kassakian, M. Schlecht, and G. C. Verghese, *Principles of Power Electronics*. Reading, MA, USA: Addison-Wesley, 1991.
[32] A. Izadian and P. Khayyer, "Application of Kalman filters in model-based fault diagnosis of a DC-DC boost converter," in *Proc. IECON 36th Annu. Conf. IEEE Ind. Electron. Soc.*, 2010, pp. 369–372.
[33] G. M. Buiatti, A. M. R. Amaral, and A. J. M. Cardoso, "An online technique for estimating the parameters of passive components in non-isolated DC/DC converters," in *Proc. IEEE Int. Symp. Ind. Electron.*, 2007, pp. 606–610.
[34] L. Palma, M. H. Todorovic, and P. N. Enjeti, "Analysis of common-mode voltage in utility-interactive fuel cell power conditioners," *IEEE Trans. Ind. Electron.*, vol. 56, no. 1, pp. 20–27, Jan. 2009.
[35] A. Santolaria, "Effects of switching frequency modulation on the power converter's output voltage," *IEEE Trans. Ind. Electron.*, vol. 56, no. 7, pp. 2729–2737, Jul. 2009.

Jun Hang (Member, IEEE) received the B.Sc. and M.Sc. degrees from Anhui University of Science and Technology, Huainan, China, in 2008 and 2011, respectively, and the Ph.D. degree from Southeast University, Nanjing, China, in 2016, all in electrical engineering.

From April 2015 to July 2015, He was a joint Ph.D. student with the Department of Energy Technology, Aalborg University, Denmark. Since 2016, he has been with Anhui University, Hefei, China, where he is currently an Associate Professor with the School of Electrical Engineering and Automation. In recent years, he has authored and coauthored more than 40 technical papers. His current research interests include condition monitoring, fault diagnosis, permanent magnet machine, and renewable energy.

Dr. Hang received the 1st Prize of 2016 Student Thesis Contest (Ph.D. Category), IEEE Industry Applications Society.

Chaoqiang Ge received the B.Sc. degree in electrical engineering and automation from Mechanical and Electrical College, Anhui Polytechnic University, Wuhu, China, in 2019. He is currently working toward the M.Sc. degree in electrical engineering with Anhui University, Hefei, China.

His current research interest includes dc–dc convert fault diagnosis.

Shichuan Ding (Member, IEEE) received the B.Sc. degree in automation from Anhui University, Hefei, China, in 2001, the M.Sc. degree in nuclear science and technology from the University of Science and Technology of China, Hefei, China, in 2006, and the Ph.D. degree in electrical engineering from Southeast University, Nanjing, China, in 2018.

Since 2001, he has been with Anhui University, where he is currently a Professor. He has been a Research Scholar with WEMPEC in University of Wisconsin Madison from April 2015 to April 2016. In recent years, he has authored and coauthored more than 40 technical papers. His research interests include electrical machine drive, power electronics applications, and energy management in EVs and in power system.

Wei Li (Member, IEEE) received the B.Sc. degree in mechanical engineering from the Anhui University of Technology, Ma'anshan, China, in 2008, the M.Sc. degree in electrical engineering from Anhui University, Hefei, China, in 2012, and the Ph.D. degree in electrical engineering from Southeast University, Nanjing, China, in 2019.

Since 2019, he has been with Anhui University, Hefei, China, where he is currently a Lecture. His current research interest includes the reliability of permanent magnet machines for application in hybrid vehicles.

Yourui Huang received the B.S. degree in automated industry from the Anhui University of Science and Technology, in 1994, and the Ph.D. degree from the Anhui Institute of Optics and Fine Mechanics, Chinese Academy of Sciences, Hefei, China, in 2000.

He is currently a Professor in control science and engineering with Anhui University of Science and Technology, Huainan, China. His research interests include intelligent information process and motion control.

Wei Hua (Senior Member, IEEE) was born in Taizhou, China, in 1978. He received the B.Sc. and Ph.D. degrees in electrical engineering from Southeast University, Nanjing, China, in 2001 and 2007, respectively.

From September 2004 to August 2005, he was with the Department of Electronics and Electrical Engineering, The University of Sheffield, U.K., as a Joint-Supervised Ph.D. student. Since 2007, he has been with Southeast University, where he is currently a Professor with the School of Electrical Engineering. He has authored or coauthored more than 150 technical papers, and he is the holder of 50 patents.